Dynamical Higgs field alignment in the NMSSM

Nina M. Coyle[1] and Carlos E. M. Wagner[1,2,3]

[1]*Physics Department and Enrico Fermi Institute, University of Chicago, Chicago, Illinois 60637, USA*
[2]*Kavli Institute for Cosmological Physics, University of Chicago, Chicago, Illinois 60637, USA*
[3]*High Energy Physics Division, Argonne National Laboratory, Argonne, Illinois 60439, USA*

(Received 20 December 2019; accepted 1 March 2020; published 30 March 2020)

Experimental probes of the recently discovered Higgs boson show that its behavior is close to that of the Standard Model (SM) Higgs particle. Extensions of the SM which include extra Higgs bosons are constrained by these observations, implying either the decoupling of the heavy nonstandard Higgs particles or the realization of alignment, associated with vanishing mixing of the SM-like Higgs boson with the nonstandard ones. Quite generally, alignment is not enforced by symmetry considerations and hence it is interesting to look for dynamical ways in which this condition can be realized. We show that this is possible in the Next-to-Minimal Supersymmetric Standard Model (NMSSM), in which alignment is achieved for values of the coupling of the Higgs fields to the singlet field that become large close to the Grand Unification (GUT) scale. This, in turn, can be explained by the composite nature of the Higgs fields, with a compositeness scale close to the GUT scale. In this article we present this dynamical scenario and discuss its phenomenological properties.

DOI: 10.1103/PhysRevD.101.055037

I. INTRODUCTION

With the discovery of the Higgs boson in 2012, the Standard Model (SM) is complete and the theory of electroweak symmetry breaking confirmed [1,2]. The primary focus of the Large Hadron Collider (LHC) since this discovery has been measurements of the precise properties of the Higgs boson [3], as well as searches for new physics. However, no evidence of new physics beyond the SM has yet been found, and the LHC Higgs boson so far appears to be SM-like.

In light of these results, extensions of the SM have become further constrained, and an interesting area of study is the examination of how extended Higgs theories may include a SM-like Higgs boson [4]. This can be achieved in two ways: either by decoupling of the nonstandard physics, rendering the SM as the effective low energy theory, or by the condition of alignment, associated with the cancellation of the mixing of the nonstandard Higgs bosons with the SM-like one. The condition of alignment has been studied in several extensions of the SM, including two Higgs doublet models, the Minimal Supersymmetric Standard Model extension (MSSM) and the next-to-minimal one (NMSSM) [4–11]. While the necessary parameter spaces have been identified and studied in the past, of further interest is the manner through which these parameter spaces may be obtained. Although in certain cases alignment may be associated with symmetry properties [12–16], this is not the case in most extensions of the SM. It is therefore of interest to study whether alignment could be achieved dynamically.

In this paper, we focus on the NMSSM and investigate how one may dynamically obtain Higgs alignment in this theory. We concentrate on the running of the NMSSM parameters up to the Grand Unification (GUT) scale, and examine general implementations of the high-energy theories suggested by such running. Particular focus is placed on Fat Higgs models, which we show may naturally include the elements necessary to satisfy the alignment limit for the doublet sector as well as limited mixing with the singlet. For this to happen, the compositeness scale must be close to the GUT scale. We therefore also examine the interesting coincidence of bottom and tau Yukawa unification at the GUT scale, which may be realized for the same parameter space as the one associated with Higgs alignment. We also consider the possibility of including a well behaved dark matter candidate within this scenario.

This paper is structured as follows. In Sec. II, we review the alignment limit of the NMSSM and the relevant conditions on the parameters necessary for alignment. In Sec. III, we present results from the running of the NMSSM parameters and examine the range of GUT-scale parameter values for which alignment is obtained in the doublet and singlet sectors. We then present an implementation of a Fat

Higgs theory which runs down to alignment at the weak scale in Sec. IV. In Sec. V, we examine the bottom- and tau-Yukawa unification for our set of low-energy parameters. Finally, in Sec. VI we present our conclusions.

II. THE ALIGNMENT LIMIT OF THE NMSSM

Within the NMSSM Higgs sector, which contains two doublets and a singlet, there are two methods through which one may obtain a SM-like Higgs of 125 GeV: decoupling and alignment. In the decoupling case, the heavier nonstandard Higgs bosons are pushed to high masses, such that the mixing with the SM-like Higgs boson is suppressed. In the case of alignment, the parameters of the Higgs sector are such that the mixing terms of the squared-mass matrix between the SM-like Higgs boson and the neutral, non-SM-like one and singlet are small. More specifically, if we work in the Higgs basis [17,18] in which only one of the doublets acquires a vacuum expectation value and hence is aligned with the SM Higgs doublet, here denoted by the subscript 1, the symmetric CP-even Higgs mass-squared matrix is given generally by

$$\mathcal{M}^2 = \begin{pmatrix} \mathcal{M}^2_{11} & \mathcal{M}^2_{12} & \mathcal{M}^2_{13} \\ & \mathcal{M}^2_{22} & \mathcal{M}^2_{23} \\ & & \mathcal{M}^2_{33} \end{pmatrix} \tag{1}$$

and the alignment condition is

$$\mathcal{M}^2_{12}, \mathcal{M}^2_{13} \ll \mathcal{O}(v^2). \tag{2}$$

With minimal mixing, we also therefore have that

$$m_h^2 \approx \mathcal{M}^2_{11} = (125\ \text{GeV})^2. \tag{3}$$

The alignment limit of the NMSSM and its phenomenological properties have previously been thoroughly investigated in Ref. [9]. Here we give a brief review of the relevant properties.

We define the relevant couplings defining the interaction of the Higgs fields through the superpotential

$$W = \lambda S H_u H_d + \frac{\kappa}{3} S^3 + h_u Q H_u U^c_R + h_d H_d Q D^c_R, \tag{4}$$

where the Higgsino mass parameter is proportional to the vacuum expectation value of the singlet field $\mu = \lambda v_s$. We shall follow the conventions of Refs. [9,19].

In the Higgs basis $\{H^{\rm SM}, H^{NSM}, H^S\}$, where $H^{\rm SM}$ denotes the SM-like Higgs, H^{NSM} the nonstandard Higgs doublet contribution and H^S the singlet contribution, the CP-even Higgs tree-level squared-mass matrix can be explicitly written as

$$\begin{pmatrix} \bar{M}_Z^2 c_{2\beta}^2 + \frac{1}{2}\lambda^2 v^2 & -\bar{M}_Z^2 s_{2\beta} c_{2\beta} & \sqrt{2}\lambda v \mu \left(1 - \frac{M_A^2}{4\mu^2} s_{2\beta}^2 - \frac{\kappa}{2\lambda} s_{2\beta}\right) \\ & M_A^2 + \bar{M}_Z^2 s_{2\beta}^2 & -\frac{1}{\sqrt{2}}\lambda v \mu c_{2\beta}\left(\frac{M_A^2}{2\mu^2} s_{2\beta} + \frac{\kappa}{\lambda}\right) \\ & & \frac{1}{4}\lambda^2 v^2 s_{2\beta}\left(\frac{M_A^2}{2\mu^2} s_{2\beta} - \frac{\kappa}{\lambda}\right) + \frac{\kappa\mu}{\lambda}\left(A_\kappa + \frac{4\kappa\mu}{\lambda}\right) \end{pmatrix} \tag{5}$$

where $s_{2\beta} = \sin 2\beta$, etc. and we have defined

$$\bar{M}_Z^2 \equiv m_Z^2 - \frac{1}{2}\lambda^2 v^2. \tag{6}$$

Including up to the first order stop loop corrections [20–27], the entries involving the doublets are given by

$$\mathcal{M}^2_{11} = \bar{M}_Z^2 c_{2\beta}^2 + \frac{1}{2}\lambda^2 v^2 + \frac{3 v^2 s_\beta^4 h_t^4}{8\pi^2}\left[\ln\left(\frac{M_S^2}{m_t^2}\right) + \frac{X_t}{M_S^2}\left(1 - \frac{X_t^2}{12 M_S^2}\right)\right] \tag{7}$$

$$\mathcal{M}^2_{22} = M_A^2 + s_{2\beta}^2\left(\bar{M}_Z^2 + \frac{3 v^2 h_t^4}{32\pi^2}\left[\ln\left(\frac{M_S^2}{m_t^2}\right) + \frac{X_t Y_t}{M_S^2}\left(1 - \frac{X_t Y_t}{12 M_S^2}\right)\right]\right) \tag{8}$$

$$\mathcal{M}^2_{12} = -s_{2\beta}\left(\bar{M}_Z^2 c_{2\beta} - \frac{3 v^2 s_\beta^2 h_t^2}{16\pi^2}\left[\ln\left(\frac{M_S^2}{m_t^2}\right) + \frac{X_t(X_t + Y_t)}{2 M_S^2} - \frac{X_t^3 Y_t}{12 M_S^4}\right]\right) \tag{9}$$

where $X_t = A_t - \mu\cot\beta$, $Y_t = A_t + \mu\tan\beta$, A_t is the stop mixing mass parameter and M_S is the geometric mean of the two stop mass eigenstates.

One may rewrite the expression for $\mathcal{M}^2_{12}$ in terms of $\mathcal{M}^2_{11}$ by relating the first-order stop loop correction terms, in which case the conditions for exact alignment up to first-order stop loop corrections become

$$\mathcal{M}_{12}^2 = \frac{1}{\tan\beta}[\mathcal{M}_{11}^2 - c_{2\beta}m_Z^2 - \lambda^2 v^2 s_\beta^2] + \frac{3v^2 s_\beta^2 h_t^4 \mu X_t}{16\pi^2 M_S^2}\left(1 - \frac{X_t^2}{6M_S^2}\right) = 0, \tag{10}$$

$$\mathcal{M}_{13}^2 = \sqrt{2}\lambda v\mu\left(1 - \frac{M_A^2 s_{2\beta}^2}{4\mu^2} - \frac{\kappa s_{2\beta}}{2\lambda}\right) = 0. \tag{11}$$

Values of the μ parameter close to the weak scale and therefore much lower than the stop masses are preferred in order to obtain a mostly bino or singlino dark matter (DM) candidate and to reduce the fine tuning associated with electroweak symmetry breaking [28,29]. As shown in Eq. (10), the stop loop corrections to $\mathcal{M}_{12}^2$ not included in $\mathcal{M}_{11}^2$ are suppressed by $\mu/M_S \ll 1$, and one may therefore neglect the stop corrections to find an approximate relation between the values of λ and $\tan\beta$ which satisfy exact alignment. Taking $\mathcal{M}_{11}^2 = m_h^2$, Eq. (10) gives [9]

$$(\lambda^A)^2 = \frac{m_h^2 - m_Z^2 c_{2\beta}}{v^2 s_\beta^2}. \tag{12}$$

Figure 1 shows the λ vs $\tan\beta$ curves given by Eq. (12) for $m_h = (125 \pm 3)$ GeV, where we have included an uncertainty of 3 GeV characterizing the theoretical uncertainties in the determination of the Higgs mass. Points within this region will be close to fulfilling exact alignment, while points close to this region should have small mixing between the two doublets. We will better define "small" mixing quantitatively in our later analyses. In order to analyze a possible dynamical origin of these parameters, we are interested in identifying the high energy-scale values

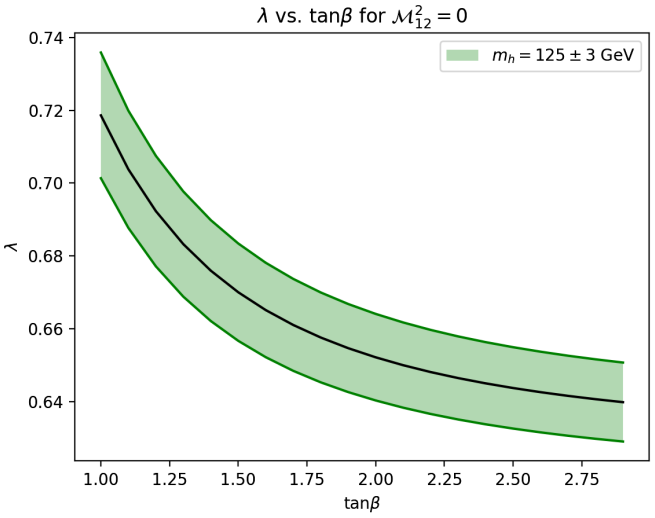

FIG. 1. λ vs $\tan\beta$ curves which gives $\mathcal{M}_{12}^2 = 0$. The solid black line shows exact alignment for $m_h = 125$ GeV. The shaded region covers $m_h = 125 \pm 3$ GeV, with the upper edge corresponding to $m_h = 128$ GeV and the lower edge to $m_h = 122$ GeV.

of NMSSM parameters which naturally run down to this alignment limit at low energies.

Although the above conditions of alignment have been derived by performing an analysis by including only one loop corrections, models that lead to an appropriate phenomenology at low energies tend to be consistent with those conditions, as shown by the similarity of the phenomenological properties of the benchmark scenarios derived in Ref. [9] compared with more complete numerical analysis as those performed in Refs. [30–44].

III. RUNNING OF NMSSM COUPLINGS TO ALIGNMENT

A. Results of running GUT-scale parameters to weak scale

As is well known, in minimal low energy supersymmetric models the values of the gauge couplings tend to evolve at a common value at a large energy scale denoted as the Grand Unification scale, $M_{\rm GUT}$, of about 2×10^{16} GeV [45–47]. The values of λ and $\tan\beta$ shown in the previous section naturally lead to large values of $\lambda(M_{\rm GUT})$ and $h_t(M_{\rm GUT})$ under the NMSSM renormalization group equations (RGE) [19]. This running seems to suggest a composite nature for the Higgs bosons, for which the relevant couplings, in this case λ and h_t, become large near the compositeness scale. In particular, if the compositeness scale is of the order of $M_{\rm GUT}$, it appears that one naturally obtains the NMSSM alignment condition $\mathcal{M}_{12}^2 = 0$ at the weak scale. Figure 2 shows the general behavior of the running of λ and h_t up to the GUT scale. In this plot, we have chosen three different points within the exact alignment region, with a low value of the nonstandard Higgs bosons masses, $M_A = 300$ GeV and a characteristic stop mass scale $M_{\rm SUSY} = 1$ TeV. Since ignoring decoupling effects $h_t(m_t) \sim m_t(m_t)/(vs_\beta)$, where m_t is the running top quark mass, the value of h_t becomes weaker at larger values of $\tan\beta$. On the other hand, taking into account decoupling effects, increases in the heavy Higgs boson scale tend to lead to somewhat lower values of h_t at the GUT-scale.

In order to thoroughly examine the range of GUT-scale parameter values for which one obtains Higgs alignment, and to identify the stability of this running to the alignment limit, we begin with a range of values for $\lambda(M_{\rm GUT})$ and $h_t(M_{\rm GUT})$ and run each pair downward in energy. There are three primary regions between M_Z and $M_{\rm GUT}$: the low-energy effective SM theory below M_A, the 2HDM region between approximately M_A and $M_{\rm SUSY}$, and the NMSSM

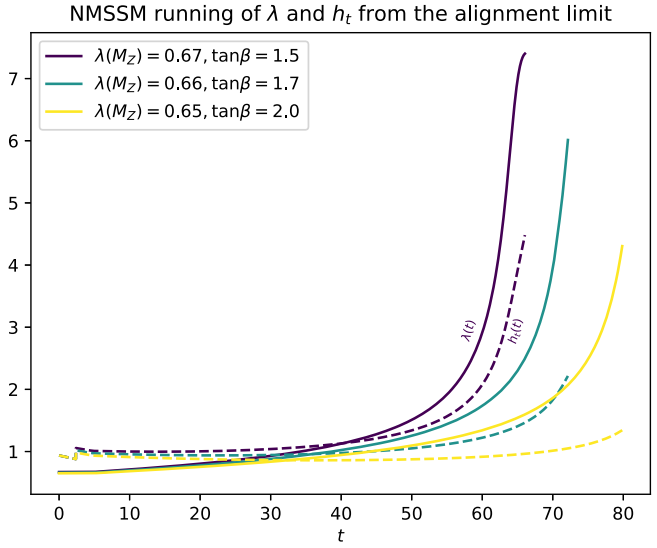

FIG. 2. Running of λ (solid lines) and h_t (dashed lines) from the weak scale to higher energies, with $t = \ln(\frac{Q^2}{M_Z^2})$. We display the running for initial values of $(\lambda(M_Z), \tan\beta) = (0.67, 1.5)$, $(0.66, 1.7)$, and $(0.65, 2.0)$, which lie within the alignment region shown in the previous section.

region above $M_{\rm SUSY}$. We employ the relevant RGE equations within each region; the equations for each region are listed in Appendix A. At the boundary between the SM and 2HDM running at M_A, we relate the single effective Higgs field in the SM to the two Higgs doublets by $\phi = H_d \cos\beta + i\tau H_u^* \sin\beta$. This relation gives $h_t^{\rm eff} = h_t \sin\beta$.

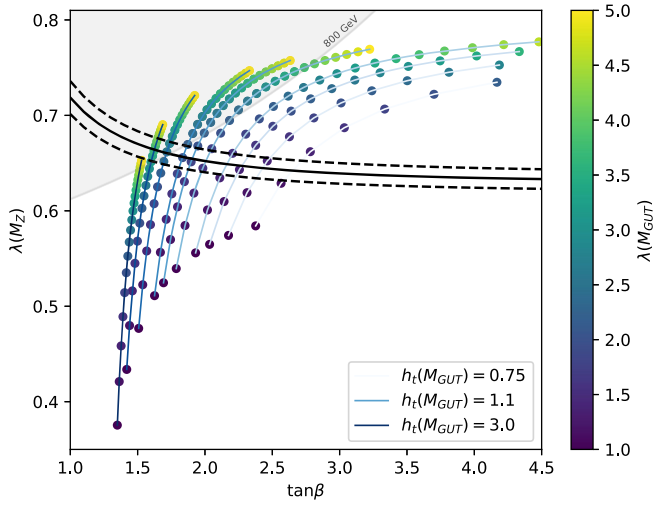

FIG. 3. Plot showing the $(\tan\beta, \lambda(M_Z))$ points obtained by running down from $M_{\rm GUT}$ with large $\lambda(M_{\rm GUT})$ and moderate $h_t(M_{\rm GUT})$. The different contours arise from varying $h_t(M_{\rm GUT})$, while the colorbar indicates the value of $\lambda(M_{\rm GUT})$. Results are displayed for $M_{\rm SUSY} = 1$ TeV. The solid and dashed black lines indicate the region of exact alignment for $m_h = 125 \pm 3$ GeV. The shaded grey region indicates the region in which it is difficult to obtain a lighter Higgs mass of 125 GeV without tension with existing stop mass limits.

We approximately identify the scale of the singlet with $M_{\rm SUSY}$, and therefore run the parameter λ between $M_{\rm GUT}$ and $M_{\rm SUSY}$, stopping its running below this scale. The value of $\tan\beta$ is determined by requiring that the running top mass is equal to approximately $m_t(M_t) \simeq 163$ GeV, leading to a pole top quark mass of approximately the observed value, $M_t \simeq 173$ GeV.

Figure 3 shows the results of running down from $M_{\rm GUT}$ to M_Z, with initial values of λ between 1 and 5 and values of h_t between 0.75 and 3.0 at the GUT scale. The value of κ is set to 0. We find that the results are stable under TeV-scale variations in the value of the running boundary $M_{\rm SUSY}$, and thus ignore the small thresholds arising from the decoupling of the supersymmetric particles. We display the results for $M_{\rm SUSY} = 1$ TeV. The value of M_A is chosen to be 300 GeV. Significantly larger values of M_A, on the order of $M_{\rm SUSY}$, push the $h_t(M_{\rm GUT}) \leq 1$ curves toward large values of $\tan\beta$. For values of $M_A \lesssim 500$ GeV, the results have little variation.

The obtention of $m_h = 125$ GeV comes into tension with existing stop mass constraints for small values of $\tan\beta$ and large values of $\lambda(M_Z)$, for which the tree level contribution to m_h becomes large. Tree-level contributions close to the observed Higgs mass result in the need for small stop loop corrections and hence small values of the stop masses [see Eq. (9)]. Based on recent results from stop searches [48–51], we use a stop mass bound of $M_S > 800$ GeV. We employ a lower bound than some of the quoted values after noting that the bounds may be relaxed depending on the specific stop decay paths and neutralino and chargino masses within the model. The scenario presented in Fig. 12 of Ref. [48] most closely aligns with the neutralino/chargino spectrum we obtain in scenarios with a realistic Dark Matter candidate, which are further discussed in Sec. IV A. Splittings between the right- and left-handed stops, multiple decay modes mediated by neutralinos and charginos, and decays through heavier Higgsinos may further relax the 800 GeV bound. In particular, we note that for lightest neutralino masses of order $m_{\tilde{\chi}_1^0} \gtrsim 200$ GeV the bounds may be relaxed significantly, and in fact no meaningful bounds are placed for $m_{\tilde{\chi}_1^0} \gtrsim 300$ GeV in that particular analysis.

Moreover, for small stop mixing, a bound on M_S is approximately equivalent from the point of view of the radiative corrections to the Higgs mass to a bound on the geometric average of the two stop masses. Hence, when comparing with experimental results one should recall that a bound $M_S > 800$ GeV is approximately equivalent to a bound on the right handed stop mass $m_{\tilde{t}_R} > 600$ GeV and on the left handed stop mass (which is close in mass to the left handed sbottom) $m_{\tilde{t}_L} > 1.1$ TeV.

From the results in Fig. 3, we see that lower values of h_t at the GUT scale tend to push $\tan\beta$ and $\lambda(M_Z)$ to larger values, while lower values of $\lambda(M_{\rm GUT})$ lead to lower values

of $\lambda(M_Z)$, as might be expected. Our points fall mostly within a range of $\lambda(M_Z) \in (0.5, 0.8)$ with moderate $\tan\beta$.

B. Alignment in the doublet sector

The points obtained from running down from large values of $\lambda(M_{\rm GUT})$, as required for a composite Higgs theory with a compositeness scale close to $M_{\rm GUT}$, fall close to the region required for exact alignment. To start with, we reduce the problem to an effective two Higgs doublet model by assuming heavy singlets and examine the mixing in the doublet sector; the suppression of the singlet mixing will be examined in the next section. To quantify how well the points fall within the alignment limit, we vary along M_S and X_t curves to examine the quantity

$$\cos(\beta-\alpha) = \frac{-\mathcal{M}_{12}^2}{\sqrt{(m_H^2-m_h^2)(m_H^2-\mathcal{M}_{11}^2)}} \tag{13}$$

which reflects the mixing between the two doublets and reduces to $-\mathcal{M}_{12}^2/(\mathcal{M}_{22}^2-\mathcal{M}_{11}^2)$ with $m_H^2 \approx \mathcal{M}_{22}^2$ and $m_h^2 \approx \mathcal{M}_{11}^2$. The M_S vs X_t curve for each $(\tan\beta, \lambda(M_Z))$ point is determined by requiring that $\mathcal{M}_{11}^2 = (125\ \text{GeV})^2$ up to the dominant two-loop terms. For low values of $\tan\beta$, the stop loop corrections tend to be smaller than the tree level values, and there is therefore little variation about the average value along each curve. As required from the choices made in the running, we use $M_A = 300$ GeV in the calculation of M_{22}^2. Larger values of M_A increase $\mathcal{M}_{22}^2$ and therefore decrease the mixing.

In the effective 2HDM, the deviations of the SM-like coupling may be parametrized by [7,8]

$$g_{hb\bar{b}} = g_{hb\bar{b}}^{\rm SM}(1-\eta) \tag{14}$$

$$g_{ht\bar{t}} = g_{ht\bar{t}}^{\rm SM}\left(1+\frac{\eta}{\tan^2\beta}\right) \tag{15}$$

$$g_{hVV} = g_{hVV}^{\rm SM}\left(1-\frac{\eta^2}{2\tan^2\beta}\right) \tag{16}$$

where

$$\eta \simeq -\tan\beta\frac{\mathcal{M}_{12}^2}{\mathcal{M}_{22}^2-\mathcal{M}_{11}^2}. \tag{17}$$

From Eqs. (14)–(16) we see that for $\tan\beta > 1$, the tree-level bottom coupling is the one mostly affected by mixing with the nonstandard states and, due to the relevant decay branching ratio of the SM-like Higgs to bottom quarks, it has a relevant effect on all Higgs branching ratios. We plot the quantity $|\eta|$, which parametrizes the variation of the bottom coupling, for our weak-scale points in Fig. 4.

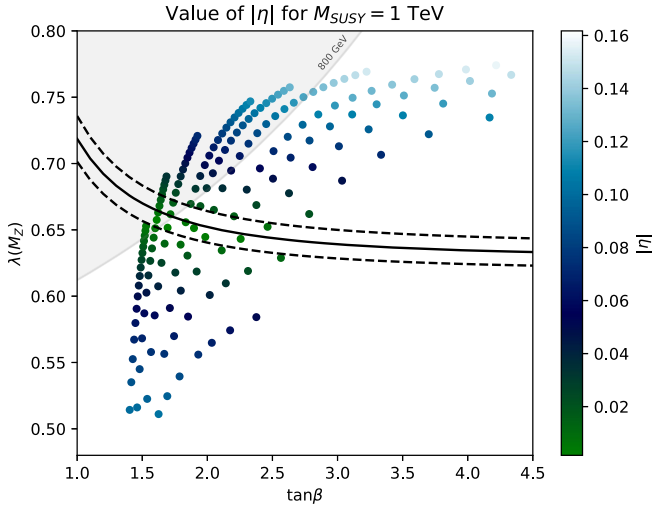

FIG. 4. Values of the quantity $|\eta|$ for the points obtained from running down from $M_{\rm GUT}$. We plot only the points which can obtain the correct Higgs mass at the 2-loop level. Points in the larger $\tan\beta$ region tend to have lower values of $\mathcal{M}_{12}^2/(\mathcal{M}_{22}^2-\mathcal{M}_{11}^2)$, but due to the larger values of $\tan\beta$ they obtain larger values of $|\eta|$ than those points at low $\tan\beta$ and λ. The shaded grey region indicates the region in which it is difficult to obtain a lighter Higgs mass of 125 GeV without tension with existing stop mass limits.

Inspection of Fig. 4 shows that the deviation of the parameter $|\eta|$ is below 0.1 for the majority of points, restricting the deviations of all couplings to values below ten percent, in agreement with current experimental observations [52–54] (in this work, we shall not consider the region in which the bottom Yukawa coupling acquires a wrong sign, $\eta \simeq 2$, which can also be achieved within the NMSSM for heavy singlets [55]). The points on the extreme ends of the $\tan\beta$ region reach larger values of $|\eta|$, but do not exceed a deviation of 0.16. Following the same analysis with a value of $M_A = 400$ GeV, we find a maximum value of $|\eta| = 0.08$, which follows the expected scaling of approximately $1/M_A^2$. We therefore find that a composite Higgs model with a compositeness scale near the GUT scale may naturally lead to the alignment limit for the doublet sector at low energies. In Sec. IV, we will describe a general implementation of an NMSSM Fat Higgs model with a scale Λ of the order of $M_{\rm GUT}$.

C. Alignment condition

As discussed above, the alignment condition in the NMSSM does not arise from a symmetry condition. To further investigate the origin of the alignment in the doublet sector, one can write the effective two Higgs doublet potential

$$V = m_{11}^2\Phi_1^\dagger\Phi_1 + m_{22}^2\Phi_2^\dagger\Phi_2 - m_{12}^2(\Phi_1^\dagger\Phi_2 + \text{H.c.}) + \frac{1}{2}\lambda_1(\Phi_1^\dagger\Phi_1)^2 + \frac{1}{2}\lambda_2(\Phi_2^\dagger\Phi_2)^2 + \lambda_3(\Phi_1^\dagger\Phi_1)(\Phi_2^\dagger\Phi_2) + \lambda_4(\Phi_1^\dagger\Phi_2)(\Phi_2^\dagger\Phi_1) + \left\{\frac{1}{2}\lambda_5(\Phi_1^\dagger\Phi_2)^2 + [\lambda_6(\Phi_1^\dagger\Phi_1) + \lambda_7(\Phi_2^\dagger\Phi_2)]\Phi_1^\dagger\Phi_2 + \text{H.c.}\right\}. \quad (18)$$

For small values of the Higgsino mass parameter compared to the stop mass scale $\mu/M_S \ll 1$—the dependence of the quartic couplings on the stop mass parameters is given, for instance, in Refs. [56,57]—one may take $\lambda_6 \simeq \lambda_7 \sim 0$ as a good approximation. The condition of alignment can then be rewritten as [7]

$$\begin{aligned} m_h^2 &= (\lambda_1\cos^4\beta + 2\tilde{\lambda}_3\sin^2\beta\cos^2\beta + \lambda_2\sin^4\beta) \\ m_h^2 &= (\lambda_1\cos^2\beta + \tilde{\lambda}_3\sin^2\beta)v^2, \end{aligned} \quad (19)$$

where $\tilde{\lambda}_3 = \lambda_3 + \lambda_4 + \lambda_5$.

In the literature, symmetry considerations have been invoked to relate the quartic couplings [12–16]. In particular, the condition $\lambda_1 = \lambda_2 = \tilde{\lambda}_3$ ensures alignment whenever $m_h^2 = \lambda_2 v^2$. In the NMSSM, however, the couplings λ_1 and λ_2 differ by the sizable stop loop corrections and these conditions cannot be fulfilled. For moderate or large values of $\tan\beta \gtrsim 2.5$, however, the alignment conditions reduce approximately to $\lambda_2 \simeq \tilde{\lambda}_3$, with $m_h^2 = \lambda_2 v^2$. Taking into account that

$$\tilde{\lambda}_3 \simeq -\frac{g_1^2 + g_2^2}{4} + \lambda^2, \quad (20)$$

one recovers the previously obtained relation, Eq. (12), which in this regime of $\tan\beta$ reads

$$\lambda^2 \simeq \frac{M_Z^2 + m_h^2}{v^2}. \quad (21)$$

Moreover, as said above, $\lambda_2 v^2$ differs from its tree-level value $M_Z^2 \simeq \lambda_1 v^2$ due to the sizable stop radiative corrections.

The relation $\lambda_2 \simeq \tilde{\lambda}_3 \simeq m_h^2/v^2$ is therefore an emergent condition arising dynamically in the infrared limit, and it is not coming from any fundamental symmetry. Alignment for smaller values of $\tan\beta$ emerges in a similar way in the infrared limit.

D. Alignment in the singlet sector

We must additionally examine how the mixing with the singlet Higgs might be naturally limited or suppressed due to the high-energy behavior of the theory. A similar analysis to the one performed for the doublet sector gives the exact alignment condition involving M_{13}^2 as

$$\frac{M_A^2 s_{2\beta}^2}{4\mu^2} - \frac{\kappa s_{2\beta}}{2\lambda} = 1. \quad (22)$$

For the region of λ and $\tan\beta$ obtained by running down from the GUT scale, the value of $\sin(2\beta)$ is approximately 1. We may thusly reduce the singlet-sector alignment condition to the approximate relation

$$\frac{M_A^2}{4\mu^2} \approx 1, \quad (23)$$

where we have assumed that $\kappa/2\lambda$ is significantly lower than one, as necessary to obtain a singlino state lighter than the Higgsino one, $2\kappa/\lambda < 1$, for which a natural dark matter candidate may be obtained [29]. Alignment for the singlet therefore additionally depends on the relationship between the parameters M_A and μ, which is not determined by the running down from M_{GUT} performed above. We therefore conclude that this alignment condition cannot obviously be imposed through choices in the high-energy theory.

We thusly examine whether one may effectively decouple the singlet due to aspects of the high-energy theory. We note that the addition of a tadpole term can effectively decouple the singlet from the doublet sector by increasing the singlet mass. In particular, the general form for $\mathcal{M}_{33}^2$ is given by [19]

$$\mathcal{M}_{33}^2 = \frac{1}{4}\lambda^2 v^2 s_{2\beta}\left(\frac{M_A^2}{2\mu^2} - \frac{\kappa}{\lambda}\right) + \frac{\kappa\mu}{\lambda}\left(A_\kappa + \frac{4\kappa\mu}{\lambda}\right) - \frac{\lambda}{\mu}\xi_S \quad (24)$$

where ξ_S is the constant in a tadpole term in the Higgs potential of the form $\xi_S S \subset V_H$. A large value of ξ_S can lead to large $\mathcal{M}_{33}^2$, thereby decoupling the singlet and limiting the mixing with the doublet sector. If the high-energy theory produces a singlet tadpole term in the Higgs potential, as we will examine in the next section, then the singlet mixing may be efficiently suppressed.

IV. FAT HIGGS MODELS

Here we focus on the possible composite nature of the Higgs, and present an example of an NMSSM Fat Higgs model [58–60] which may run down to alignment at the weak scale as examined in the previous section. The primary traits we require are large values of λ at the GUT scale and a singlet tadpole term which may decouple the singlet from mixing with the doublet sector. We therefore choose a

compositeness scale of $\Lambda_H \approx M_{\rm GUT} \approx 10^{16}$ GeV, and include a supersymmetric mass term for the two new superfields which form the singlet at low energies, thereby generating a tadpole term for S.

We specifically follow the construction set forth by Harnik *et al.* in Ref. [58], which presents an NMSSM Fat Higgs model. A new gauge symmetry $SU(2)_H$ is introduced, which becomes strong at a scale Λ_H, and six new superfields $T^{1,\ldots 6}$ are introduced which are doublets under $SU(2)_H$. (T_1, T_2) also transform as a doublet under $SU(2)_L$, while (T_3, T_4) and (T_5, T_6) transform as singlets under $SU(2)_L$. The tree-level superpotential is given by

$$W = yS'T^1T^2 + yS''T^3T^4 - mT^5T^6 + \cdots \tag{25}$$

where S' and S'' are new singlet superfields included to ensure dynamic electroweak symmetry breaking. Making the identifications

$$S \propto T^5T^6, \quad \begin{pmatrix} H_u^+ \\ H_u^0 \end{pmatrix} \propto \begin{pmatrix} T^1T^3 \\ T^2T^3 \end{pmatrix}, \quad \begin{pmatrix} H_d^0 \\ H_d^- \end{pmatrix} \propto \begin{pmatrix} T^1T^4 \\ T^2T^4 \end{pmatrix} \tag{26}$$

one obtains a dynamically generated superpotential of

$$W = \lambda S(H_uH_d - v_0^2). \tag{27}$$

Using naive dimensional analysis [61–64], one expects that

$$v_0^2 \sim \frac{m\Lambda_H}{(4\pi)^2} \tag{28}$$

$$\lambda(\Lambda_H) \sim 4\pi. \tag{29}$$

Of particular interest in our case is the very small value of m required to obtain $v_0 \approx \mathcal{O}(100)$ GeV for a compositeness scale of $\Lambda_H \approx 10^{16}$ GeV; in particular, m must be on the order of 10^{-1} eV.

We note that a term of the form mT^5T^6 may arise from the vev of a scalar superfield, in which case one would have a term of the form $g\Phi T^5T^6$, where g is a dimensionless coupling. As a scalar superfield, Φ may have the form $\Phi = \varphi + \theta\theta F$, where φ and F have some vacuum expectation values. When integrating to obtain the potential, one therefore finds an additional term linear in the Higgs singlet S arising from the F-term. Thus, the presence of a tadpole term of the form $\xi_F\hat{S}$ in the superpotential may naturally give rise to a tadpole term in the potential of the form $\xi_S S$.

The necessary scales can be estimated based on the values of m we require due to the compositeness scale, as well as the scale of ξ_S required to decouple the singlet from the doublet sector. We write the Higgs singlet terms with the vev of $\langle\Phi\rangle = \langle\varphi\rangle + \theta\theta\langle F_\phi\rangle$ by

$$g(\langle\varphi\rangle + \theta\theta\langle F_\varphi\rangle)T^5T^6 \tag{30}$$

where the first term generates the supersymmetric mass term mT^5T^6 while the second term generates the tadpole term in the potential. We estimate that $\langle\varphi\rangle$ and $\sqrt{|\langle F\rangle|}$ should both be on the order of a TeV. In order to obtain $m \sim \mathcal{O}(10^{-1})$ eV, we therefore require $g \sim \mathcal{O}(10^{-13})$. The scalar part of $\hat{S}$ then acquires a tadpole term in the potential with $\xi_S = \frac{\Lambda_H g\langle F\rangle}{4\pi}$; we require ξ_S on the order of 10^9 GeV^3 for decoupling, which indicates that Λ_H is around 10^{15} GeV. We thus obtain a similar compositeness scale to the one that matches the NMSSM running, as described in Sec. III.

The problem now reduces to the generation of the small coupling g. Such a small coupling may be explained by using a seesaw mechanism, similar to the one associated with the Majorana neutrino mass models. In order to propose such a model, let us follow Ref. [58] and introduce two additional $SU(2)_H$ doublets T^7 and T^8. We shall assume the presence of certain flavor symmetries which forbid an explicit T^5T^6 mass term, but allow mixing between these states and the T^7 and T^8 term via the analogue of a Giudice Masiero mechanism [65] and a T^7T^8 mass term via the interaction with an additional superfield, Ψ. Under these assumptions, the superpotential reads

$$W = \Psi T^7T^8 + m_{\rm SUSY}T^5T^8 + m_{\rm SUSY}T^6T^7 \tag{31}$$

where the $m_{\rm SUSY}$ term comes from the Giudice Masiero relation between the effective bilinear superfield term and the supersymmetry breaking scale. We shall assume that

$$\langle\Psi\rangle \simeq M + F\theta^2 \tag{32}$$

where F is proportional to the square of the supersymmetry breaking scale, such that the superpartner masses $m_{\rm SUSY} \simeq F/M_{\rm GUT}$, and M is of the order of the GUT scale. Integrating out the heavy superfields T^7 and T^8, one can identify the supersymmetry conserving and breaking terms that appear at low energies. This can be done diagrammatically. For instance, the supersymmetry breaking tadpole term may be obtained by considering the presence of the scalar mixing terms in the scalar potential,

$$V \simeq M^2(T_7T_7^* + T_8T_8^*) + m_{\rm SUSY}M(T_5T_7^* + T_6T_8^*) + FT_7T_8 + \text{H.c.}, \tag{33}$$

where the first four terms arise from F terms in the superpotential, of the form $|\partial W/\partial T_7|^2$ and $|\partial W/\partial T_8|^2$, and we replace Ψ by its vacuum expectation value. After integrating out the heavy fields, the above terms lead to a supersymmetry breaking term

$$V \simeq m_{\mathrm{SUSY}}^2 \frac{F}{M^2} T_5 T_6 + \mathrm{H.c.} \tag{34}$$

This induces a tadpole of the right size for the scalar component of S.

Alternatively, one can also obtain the same result by doing a simple expansion considering the supersymmetry breaking terms like a perturbation of the values obtained in the supersymmetric limit. Let us start with the supersymmetric case, with superpotential

$$W = M T^7 T^8 + m_{\mathrm{SUSY}} T^5 T^8 + m_{\mathrm{SUSY}} T^6 T^7. \tag{35}$$

Integrating out the heavy superfields, we get the effective superpotential

$$W = -\frac{m_{\mathrm{SUSY}}^2}{M} T_5 T_6. \tag{36}$$

This term, together with the supersymmetry breaking term, Eq. (34), leads to the supersymmetric and nonsupersymmetric tadpole contributions of the singlet S. We can then formally identify the spectator field Φ introduced in Eq. (30) with

$$g\langle\Phi\rangle \simeq -\frac{m_{\mathrm{SUSY}}^2}{\langle\Psi\rangle}, \tag{37}$$

where the above expression acquires meaning after decoupling the heavy superfields T^7, T^8 and performing the above mentioned expansion [66], from which we obtain

$$\begin{aligned} g &\simeq -\frac{m_{\mathrm{SUSY}}}{M}, \\ \langle\Phi\rangle &= m_{\mathrm{SUSY}} - \frac{m_{\mathrm{SUSY}} F}{M}\theta^2 \sim m_{\mathrm{SUSY}} - m_{\mathrm{SUSY}}^2 \theta^2. \end{aligned} \tag{38}$$

Hence, we reproduce the diagrammatic result for the supersymmetry breaking tadpole and obtain the required values of the coupling and the effective superfield Φ vacuum expectation values in a natural way.

While the interactions of the singlet field S with the Higgs field have the required structure to obtain alignment, the self interactions of S are not determined in a clear way from our discussion above. We shall assume that the flavor symmetries forbid a superpotential mass term for S but allow the presence of a cubic term in S, induced by strong interactions at the scale M and characterized by the usual κ term at low energies. As shown in Appendix B, provided κ acquires moderate values there is no modification of the range of values of λ obtained in the running.

A. Phenomenological properties

The low energy limit of the model presented above is equivalent to the $\mathbb{Z}_3$ invariant NMSSM, with the addition of tadpole terms that lift the scalar components of the singlet fields to values larger than the weak scale, implying the suppression of the mixing of the singlet with the SM Higgs bosons. Moreover, the values of λ ensure approximate alignment in the doublet Higgs sector. The combination of alignment in the doublet Higgs sector with the decoupling of the singlet scalar fields imply that the observed Higgs boson has approximate Standard Model-like properties, in agreement with experiments.

This model does not predict the exact value of the nonstandard Higgs boson masses, but the moderate values of $\tan\beta$ imply that the production cross section is governed by top-Yukawa induced processes. Due to the alignment condition, which suppresses the decay into pairs of weak gauge bosons or SM-like Higgs bosons [9], and the absence of light singlets, the nonstandard Higgs bosons decay mostly into fermion states. Therefore, the decay branching ratio depends on whether the decay into pairs of top-quarks and electroweakinos is allowed. If top-quark decay is dominant, searches for the heavy Higgs doublets become difficult due to interference effects with the large top-quark production background [67–71]. Therefore, the only region that is currently constrained is for low values of $\tan\beta < 2$ and values of the heavy Higgs mass below about 350 GeV, where the top-quark decay process is absent. The main constraint comes from the decay of the heavy Higgs bosons into τ pairs [72,73] which, however, can be efficiently suppressed if the electroweakinos are light [74].

Regarding the chargino and neutralino sectors, the model provides an acceptable dark matter candidate in terms of the lightest neutralino [19]. Assuming this particle to be either predominantly bino or singlino, spin independent direct detection bounds may be efficiently suppressed provided [29]

$$m_\chi \sim \pm\mu \sin 2\beta, \tag{39}$$

where the plus sign corresponds to the singlino case, while the minus sign corresponds to the bino case. However, the suppression of the direct detection cross section in the singlino case relies on the interference between the SM-like and singlet scalar Higgs contributions, which requires a light scalar singlet. In the case of singlet decoupling, it is difficult to obtain a small direct detection cross section. However, the bino case remains viable under direct detection limits. Moreover, values of the singlino mass close to the bino mass and somewhat lower than the Higgsino mass μ ensure the obtention of the proper relic density via co-annihilation of the bino with the singlino. An acceptable relic density may therefore be obtained consistently with the condition of avoiding the direct detection bounds in this model. Using NMSSMTools [75] we have verified that one may indeed

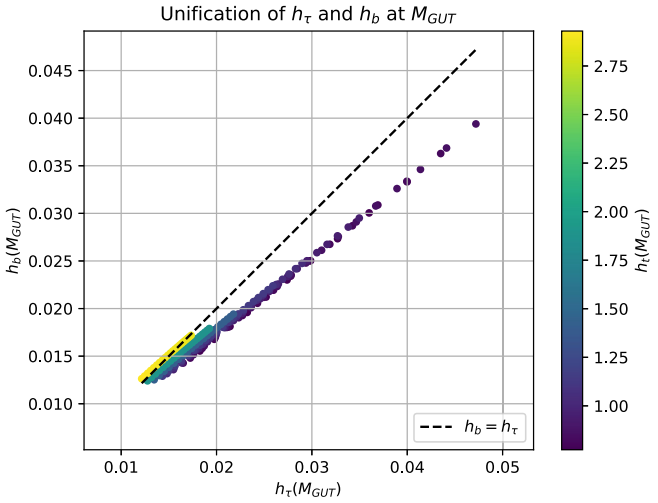

FIG. 5. Plot of the values of $h_\tau(M_{\rm GUT})$ and $h_b(M_{\rm GUT})$ obtained from running the weak-scale points shown in Fig. 3 up to the GUT scale. The color bar indicates the value of $h_t(M_{\rm GUT})$, for which larger values push the values of h_τ and h_b closer to unification at the GUT scale.

obtain approximate alignment with an acceptable dark matter candidate, for instance for $\tan\beta \simeq 2.5$ and $\lambda(M_Z) \simeq 0.69$ with values of $M_1 = 240$ GeV, $M_A \simeq 400$ GeV and $\mu = -300$ GeV, $\kappa \simeq 0.33$ and $M_S \simeq 800$ GeV (or equivalently $m_{\tilde{t}_R} \simeq 600$ GeV and $m_{\tilde{t}_L} \simeq 1.1$ TeV).

A further phenomenological consideration is the charged Higgs contribution to the $b \to s\gamma$ rate. Within a basic Type II 2HDM model, a light charged Higgs on the order of a few hundred GeV enhances $b \to s\gamma$ rates and therefore becomes constrained by experimental measurements [76–79]. However, within supersymmetric theories these flavor rates also depend strongly on the contributions from other supersymmetric particles; these include charginos and stops, which can exactly cancel the SM contributions to the $b \to s\gamma$ transition in the limit of exact supersymmetry [80–83]. Furthermore, there are contributions arising from possible flavor violation in the scalar fermion sector; these can be large corrections arising from gluino-squark loops. This can occur when there is a misalignment between the bases in which the quark and squark mass matrices are diagonalized [84]. In light of this, we do not further consider flavor constraints; however, we have confirmed using NMSSMTools that the models described above can be in agreement with flavor constraints up to the SUSY contributions included in NMSSMTools.

V. UNIFICATION OF h_b AND h_τ

Although it is not directly related to the alignment in the Higgs sector, another intriguing aspect of the running of the RG evolution from the alignment limit is the unification of h_b and h_τ at the GUT scale. Figure 5 shows the values of $h_b(M_{\rm GUT})$ and $h_\tau(M_{\rm GUT})$ obtained by running the weak-scale points in Fig. 3 upward to the GUT scale. As expected from previous work [85–96], for such large values of $h_t(M_{\rm GUT})$ the values approach the $h_b(M_{\rm GUT}) = h_\tau(M_{\rm GUT})$ line as h_t increases. The values of h_t approach an infrared fixed point [87], which is also a feature of top condensate models [97–99], which is a different realization of compositeness in the Higgs doublet sector.

The unification of the bottom and tau Yukawa couplings suggests that the bottom-quark and τ-lepton share the same representations of the high-energy theory, as would happen in an effective $SU(5)$ theory at the GUT scale. However, GUT scenarios tend to encounter a number of phenomenological issues (see, for example, Refs. [100–104]), and an examination of how one may build a successful Grand Unification theory with the NMSSM as the low-energy theory, along with composite Higgs bosons, is beyond the scope of this paper.

VI. CONCLUSION

The condition of alignment in the Higgs sector allows for the possibility of obtaining a relatively light Higgs spectrum without being in conflict with the LHC Higgs precision measurements. Quite generally, alignment is not dictated by any symmetry consideration and, barring the possibility of being an accidental condition, requires a dynamical explanation. In this article we concentrated on the NMSSM, in which the alignment condition is associated with a narrow range of values of the superpotential coupling λ, which governs the interactions of the singlet to doublet Higgs states. For low values of $\tan\beta \lesssim 3$, this range of values of λ leads to the observed value of the Higgs mass without requiring a very large stop spectrum. Moreover, as shown in this article, the renormalization group evolution of the coupling λ shows that for low energy values which lead to alignment in the Higgs sector, λ tends to become strong at scales of the order of the GUT scale. Furthermore, the top Yukawa coupling also tends to large values at similar large energy scales.

In this article we interpret the large values of λ at the GUT scale as a signal of compositeness of the Higgs states. Following this idea, we construct a Fat Higgs model with a compositeness scale that is close to the GUT scale, which leads to the desired Higgs spectrum and allows for the presence of a tadpole contribution that leads to the natural decoupling of the singlet scalar states in the low energy theory. This implies that the alignment in the doublet sector, governed by λ, ensures the SM-like properties of the lightest Higgs, as required by the LHC precision measurements.

In addition to obtaining a Higgs sector which is consistent with current experimental constraints, the model also includes a dark matter candidate, which is mostly binolike and obtains the correct relic density through coannihilation with light singlinos. Moreover, for values

of the dark matter mass close to $-\mu \sin 2\beta$, direct detection constraints can be avoided in the bino case. All these conditions may be simultaneously satisfied within these models.

Finally, we stress that the relatively strong values of the top Yukawa coupling lead to the unification of the bottom and tau Yukawa couplings at the GUT scale. This suggests the possible embedding of this theory within a GUT scenario, like $SU(5)$, in which the bottom-quark and tau-lepton share the same multiplets. We reserve for future work the construction of such a theory.

ACKNOWLEDGMENTS

We thank Timothy Tait, Antonio Delgado, Nausheen Shah, and Roni Harnik for useful discussions. Work at A. N. L. is supported in part by the U.S. Department of Energy under Contract No. DE-AC02-06CH11357. The work of C. W. and N. C. at E. F. I. is supported by the U.S. Department of Energy under Contract No. DE-FG02-13ER41958. Work by N. C. at F. N. A. L. is supported by the U.S. Department of Energy, Office of Science, Office of Workforce Development for Teachers and Scientists, Office of Science Graduate Student Research (SCGSR) program. The SCGSR program is administered by the Oak Ridge Institute for Science and Education (ORISE) for the DOE. ORISE is managed by ORAU under Contract No. DE-SC0014664.

APPENDIX A: RGE EQUATIONS

We list here the RGE equations used for the running of the couplings presented in Sec. III.

1. SM and 2HDM

The equations used for the Standard Model and 2HDM running are given by [105]

$$\begin{aligned}
\frac{d\alpha_3}{dt} &= 7\frac{\alpha_3^2}{4\pi} \\
\frac{d\alpha_2}{dt} &= \beta_2\frac{\alpha_2^2}{4\pi} \\
\frac{d\alpha_1}{dt} &= -\beta_1\frac{\alpha_1^2}{4\pi} \\
\frac{dY_t}{dt} &= Y_t\left(8\tilde{\alpha}_3 + \frac{9}{4}\tilde{\alpha}_2 + \frac{17}{12}\tilde{\alpha}_1 - \frac{9}{2}Y_t - \frac{\alpha_b}{2}Y_b - \alpha_\tau Y_\tau\right) \\
\frac{dY_b}{dt} &= Y_b\left(8\tilde{\alpha}_3 + \frac{9}{4}\tilde{\alpha}_2 + \frac{5}{12}\tilde{\alpha}_1 - \frac{9}{2}Y_b - \frac{\alpha_t}{2}Y_t - Y_\tau\right) \\
\frac{dY_\tau}{dt} &= Y_\tau\left(\frac{9}{4}\tilde{\alpha}_2 + \frac{15}{4}\tilde{\alpha}_1 - \frac{5}{2}Y_\tau - 3Y_b - \alpha_t' Y_t\right)
\end{aligned} \tag{A1}$$

where $\alpha_i = g_i^2/4\pi$, $\tilde{\alpha}_i = \alpha_i/4\pi$, $Y_{t,b} = h_{t,b}^2/16\pi^2$, and $t = \log(M_{\rm GUT}^2/\mu^2)$. The parameters $(\beta_2, \beta_1, \alpha_b, \alpha_t, \alpha_t', \alpha_\tau)$ are equal to (3,7,1,1,0,0) for the 2HDM and $(19/6, 41/6, 3, 3, 3, 1)$ for the SM running.

2. NMSSM

The 2-loop RGE [19] used for the NMSSM running are listed below; we employ the SM normalization of g_1. The running parameter t is defined here as $t = \ln(Q^2/M_Z^2)$.

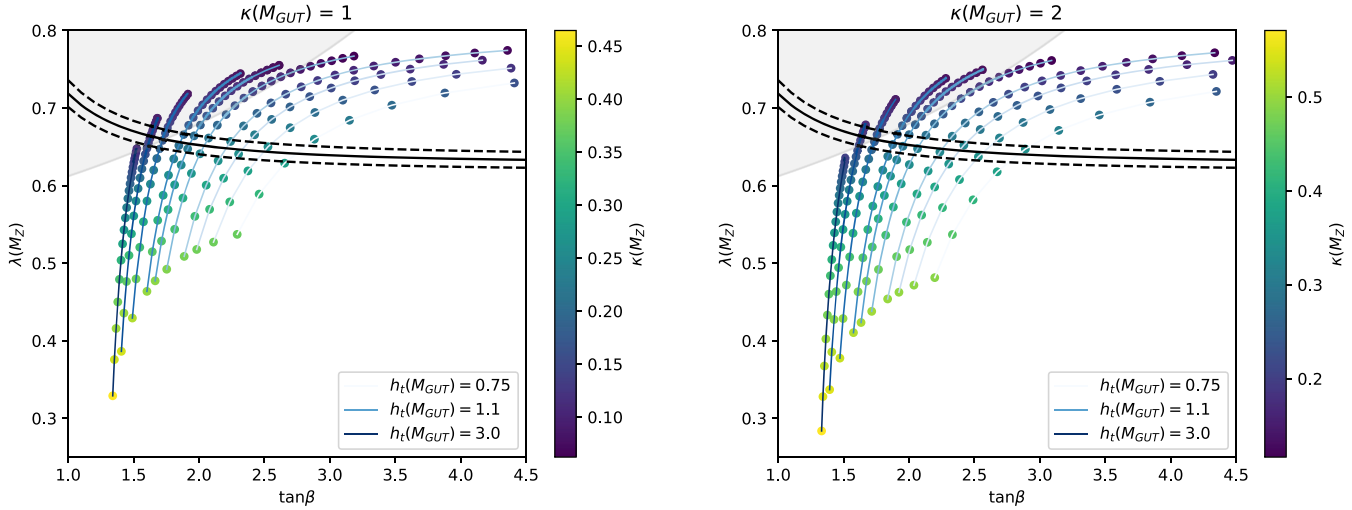

FIG. 6. Plots showing the points obtained from running down from the GUT scale with different values of $\kappa(M_{\rm GUT})$. All other parameter choices, including the ranges of $\lambda(M_{\rm GUT})$ and $h_t(M_{\rm GUT})$, are the same as for Fig. 3.

$$
\begin{aligned}
16\pi^2\frac{dg_1^2}{dt} &= 11g_1^4 + \frac{g_1^4}{16\pi^2}\left(\frac{199}{9}g_1^2 + 9g_2^2 + \frac{88}{3}g_3^2 - \frac{26}{3}h_t^2 - \frac{14}{3}h_b^2 - 6h_\tau^2 - 2\lambda^2\right)\\
16\pi^2\frac{dg_2^2}{dt} &= g_2^4 + \frac{g_2^4}{16\pi^2}(3g_1^2 + 25g_2^2 + 24g_3^2 - 6h_t^2 - 6h_b^2 - 2h_\tau^2 - 2\lambda^2)\\
16\pi^2\frac{dg_3^2}{dt} &= -3g_3^4 + \frac{g_3^4}{16\pi^2}\left(\frac{11}{3}g_1^2 + 9g_2^2 + 14g_3^2 - 4h_t^2 - 4h_b^2\right)\\
16\pi^2\frac{dh_t^2}{dt} &= h_t^2\left(6h_t^2 + h_b^2 + \lambda^2 - \frac{13}{9}g_1^2 - 3g_2^2 - \frac{16}{3}g_3^2\right)\\
&\quad + \frac{h_t^2}{16\pi^2}\left(-22h_t^4 - 5h_b^4 - 3\lambda^4 - 5h_t^2h_b^2 - 3h_t^2\lambda^2 - h_b^2h_\tau^2 - 4h_b^2\lambda^2\right.\\
&\quad - h_\tau^2\lambda^2 - 2\lambda^2\kappa^2 + 2g_1^2h_t^2 + \frac{2}{3}g_1^2h_b^2 + 6g_2^2h_t^2 + 16g_3^2h_t^2\\
&\quad \left. + \frac{2743}{162}g_1^4 + \frac{15}{2}g_2^4 - \frac{16}{9}g_3^4 + \frac{5}{3}g_1^2g_2^2 + \frac{136}{27}g_1^2g_3^2 + 8g_2^2g_3^2\right)\\
16\pi^2\frac{dh_b^2}{dt} &= h_b^2\left(6h_b^2 + h_t^2 + h_\tau^2 + \lambda^2 - \frac{7}{9}g_1^2 - 3g_2^2 - \frac{16}{3}g_3^2\right)\\
&\quad + \frac{h_b^2}{16\pi^2}\left(-22h_b^4 - 5h_t^4 - 3h_\tau^4 - 3\lambda^4 - 5h_b^2h_t^2 - 3h_b^2h_\tau^2 - 3h_b^2\lambda^2\right.\\
&\quad - 4h_t^2\lambda^2 - 2\lambda^2\kappa^2 + \frac{2}{3}g_1^2h_b^2 + \frac{4}{3}g_1^2h_t^2 + 2g_1^2h_\tau^2 + 6g_2^2h_b^2 + 16g_3^2h_b^2\\
&\quad \left. + \frac{1435}{162}g_1^4 + \frac{15}{2}g_2^4 - \frac{16}{9}g_3^4 + \frac{5}{3}g_1^2g_2^2 + \frac{40}{27}g_1^2g_3^2 + 8g_2^2g_3^2\right)\\
16\pi^2\frac{dh_\tau^2}{dt} &= h_\tau^2(4h_\tau^2 + 3h_b^2 + \lambda^2 - 3g_1^2 - 3g_2^2)\\
&\quad + \frac{h_\tau^2}{16\pi^2}\left(-10h_\tau^4 - 9h_b^4 - 3\lambda^4 - 9h_\tau^2h_b^2 - 3h_\tau^2\lambda^2 - 3h_t^2h_b^2 - 3h_t^2\lambda^2\right.\\
&\quad \left. - 2\lambda^2\kappa^2 + 2g_1^2h_\tau^2 - \frac{2}{3}g_1^2h_b^2 + 6g_2^2h_\tau^2 + 16g_3^2h_b^2 + \frac{75}{2}g_1^4 + \frac{15}{2}g_2^4 + 3g_1^2g_2^2\right)\\
16\pi^2\frac{d\lambda^2}{dt} &= \lambda^2(3h_t^2 + 3h_b^2 + h_\tau^2 + 4\lambda^2 + 2\kappa^2 - g_1^2 - 3g_2^2)\\
&\quad + \frac{\lambda^2}{16\pi^2}\left(-10\lambda^4 - 9h_t^4 - 9h_b^4 - 3h_\tau^4 - 8\kappa^4 - 9\lambda^2h_t^2 - 9\lambda^2h_b^2\right.\\
&\quad - 3\lambda^2h_\tau^2 - 12\lambda^2\kappa^2 - 6h_t^2h_b^2 + 2g_1^2\lambda^2 + \frac{4}{3}g_1^2h_t^2 - \frac{2}{3}g_1^2h_b^2 + 2g_1^2h_\tau^2\\
&\quad \left. + 6g_2^2\lambda^2 + 16g_3^2h_t^2 + 16g_3^2h_b^2 + \frac{23}{2}g_1^4 + \frac{15}{2}g_2^4 + 3g_1^2g_2^2\right)\\
16\pi^2\frac{d\kappa^2}{dt} &= \kappa^2(6\lambda^2 + 6\kappa^2) + \frac{\kappa^2}{16\pi^2}(-24\kappa^4 - 12\lambda^4 - 24\kappa^2\lambda^2\\
&\quad - 18h_t^2\lambda^2 - 18h_b^2\lambda^2 - 6h_\tau^2\lambda^2 + 6g_1^2\lambda^2 + 18g_2^2\lambda^2)
\end{aligned}
$$

APPENDIX B: RESULTS FOR NONZERO κ

In the main analysis of this paper, we set $\kappa = 0$; in this section we present results for different values of κ at the GUT scale to quantify the effect of a nonzero value of κ on the results of the running. In Fig. 6 we plot the results of running downward for $\kappa(M_{\rm GUT}) = 1, 2$ with $M_{\rm SUSY} = 1$ TeV.

The large values of $\kappa(M_{\rm GUT})$ do not significantly affect the weak-scale parameter values, which remain near the alignment region. The primary effect of increased κ is a lower value of $\lambda(M_Z)$, which tends to be reduced by up to about 0.05 relative to the $\kappa = 0$ case. Based on the low variation in the results with large κ, we conclude that setting $\kappa = 0$ provides a representative analysis.

[1] G. Aad *et al.* (ATLAS Collaboration), Phys. Lett. B **716**, 1 (2012).
[2] S. Chatrchyan *et al.* (CMS Collaboration), Phys. Lett. B **716**, 30 (2012).
[3] G. Aad *et al.* (ATLAS and CMS Collaborations), Phys. Rev. Lett. **114**, 191803 (2015).
[4] J. F. Gunion and H. E. Haber, Phys. Rev. D **67**, 075019 (2003).
[5] A. Delgado, G. Nardini, and M. Quiros, J. High Energy Phys. 07 (2013) 054.
[6] N. Craig, J. Galloway, and S. Thomas, arXiv:1305.2424.
[7] M. Carena, I. Low, N. R. Shah, and C. E. M. Wagner, J. High Energy Phys. 04 (2014) 015.
[8] M. Carena, H. E. Haber, I. Low, N. R. Shah, and C. E. M. Wagner, Phys. Rev. D **91**, 035003 (2015).
[9] M. Carena, H. E. Haber, I. Low, N. R. Shah, and C. E. M. Wagner, Phys. Rev. D **93**, 035013 (2016).
[10] J. Bernon, J. F. Gunion, H. E. Haber, Y. Jiang, and S. Kraml, Phys. Rev. D **92**, 075004 (2015).
[11] H. E. Haber, S. Heinemeyer, and T. Stefaniak, Eur. Phys. J. C **77**, 742 (2017).
[12] P. S. B. Dev and A. Pilaftsis, J. High Energy Phys. 12 (2014) 024.
[13] P. S. Bhupal Dev and A. Pilaftsis, J. Phys. Conf. Ser. **873**, 012008 (2017).
[14] K. Benakli, M. D. Goodsell, and S. L. Williamson, Eur. Phys. J. C **78**, 658 (2018).
[15] K. Benakli, Y. Chen, and G. Lafforgue-Marmet, Eur. Phys. J. C **79**, 172 (2019).
[16] N. Darvishi and A. Pilaftsis, Phys. Rev. D **99**, 115014 (2019).
[17] H. Georgi and D. V. Nanopoulos, Phys. Lett. B **82**, 95 (1979); J. F. Donoghue and L. F. Li, Phys. Rev. D **19**, 945 (1979); L. Lavoura and J. P. Silva, Phys. Rev. D **50**, 4619 (1994); L. Lavoura, Phys. Rev. D **50**, 7089 (1994); F. J. Botella and J. P. Silva, Phys. Rev. D **51**, 3870 (1995).
[18] See Chapter 22 of G. C. Branco, L. Lavoura, and J. P. Silva, *CP Violation* (Oxford University Press, Oxford, 1999).
[19] U. Ellwanger, C. Hugonie, and A. M. Teixeira, Phys. Rep. **496**, 1 (2010).
[20] H. E. Haber and R. Hempfling, Phys. Rev. Lett. **66**, 1815 (1991); Y. Okada, M. Yamaguchi, and T. Yanagida, Prog. Theor. Phys. **85**, 1 (1991); J. R. Ellis, G. Ridolfi, and F. Zwirner, Phys. Lett. B **257**, 83 (1991).
[21] H. E. Haber and R. Hempfling, Phys. Rev. D **48**, 4280 (1993).
[22] See e.g., M. Carena, H. E. Haber, S. Heinemeyer, W. Hollik, C. E. M. Wagner, and G. Weiglein, Nucl. Phys. **B580**, 29 (2000); G. Degrassi, S. Heinemeyer, W. Hollik, P. Slavich, and G. Weiglein, Eur. Phys. J. C **28**, 133 (2003).
[23] G. F. Giudice and A. Strumia, Nucl. Phys. **B858**, 63 (2012).
[24] E. Bagnaschi, G. F. Giudice, P. Slavich, and A. Strumia, J. High Energy Phys. 09 (2014) 092.
[25] P. Draper, G. Lee, and C. E. M. Wagner, Phys. Rev. D **89**, 055023 (2014).
[26] J. P. Vega and G. Villadoro, J. High Energy Phys. 07 (2015) 159.
[27] G. Lee and C. E. M. Wagner, Phys. Rev. D **92**, 075032 (2015).
[28] C. Brust, A. Katz, S. Lawrence, and R. Sundrum, J. High Energy Phys. 03 (2012) 103.
[29] S. Baum, M. Carena, N. R. Shah, and C. E. M. Wagner, J. High Energy Phys. 04 (2018) 069.
[30] U. Ellwanger, J. High Energy Phys. 03 (2012) 044.
[31] J. F. Gunion, Y. Jiang, and S. Kraml, Phys. Lett. B **710**, 454 (2012).
[32] S. F. King, M. Muhlleitner, and R. Nevzorov, Nucl. Phys. **B860**, 207 (2012).
[33] J. J. Cao, Z. X. Heng, J. M. Yang, Y. M. Zhang, and J. Y. Zhu, J. High Energy Phys. 03 (2012) 086.
[34] D. A. Vasquez, G. Belanger, C. Boehm, J. Da Silva, P. Richardson, and C. Wymant, Phys. Rev. D **86**, 035023 (2012).
[35] U. Ellwanger and C. Hugonie, Adv. High Energy Phys. **2012**, 625389 (2012).
[36] K. Agashe, Y. Cui, and R. Franceschini, J. High Energy Phys. 02 (2013) 031.
[37] K. Kowalska, S. Munir, L. Roszkowski, E. M. Sessolo, S. Trojanowski, and Y. L. S. Tsai, Phys. Rev. D **87**, 115010 (2013).
[38] S. F. King, M. Mhlleitner, R. Nevzorov, and K. Walz, Nucl. Phys. **B870**, 323 (2013).
[39] T. Gherghetta, B. von Harling, A. D. Medina, and M. A. Schmidt, J. High Energy Phys. 02 (2013) 032.
[40] R. Barbieri, D. Buttazzo, K. Kannike, F. Sala, and A. Tesi, Phys. Rev. D **87**, 115018 (2013).
[41] M. Badziak, M. Olechowski, and S. Pokorski, J. High Energy Phys. 06 (2013) 043.
[42] U. Ellwanger, J. High Energy Phys. 08 (2013) 077.
[43] F. Domingo and G. Weiglein, J. High Energy Phys. 04 (2016) 095.
[44] S. F. King, M. Mühlleitner, R. Nevzorov, and K. Walz, Phys. Rev. D **90**, 095014 (2014).
[45] J. R. Ellis, S. Kelley, and D. V. Nanopoulos, Phys. Lett. B **260**, 131 (1991).
[46] P. Langacker and M. x. Luo, Phys. Rev. D **44**, 817 (1991).

[47] U. Amaldi, W. de Boer, and H. Furstenau, Phys. Lett. B **260**, 447 (1991).
[48] M. Aaboud *et al.* (ATLAS Collaboration), J. High Energy Phys. 12 (2017) 085.
[49] M. Aaboud *et al.* (ATLAS Collaboration), J. High Energy Phys. 06 (2018) 108.
[50] CMS Collaboration, CERN Report No. CMS-PAS-SUS-19-009, 2019.
[51] ATLAS Collaboration, CERN Report No. ATLAS-CONF-2019-017, 2019.
[52] ATLAS Collaboration, CERN Report No. ATLAS-CONF-2018-031, 2018.
[53] A. M. Sirunyan *et al.* (CMS Collaboration), Eur. Phys. J. C **79**, 421 (2019).
[54] G. Aad *et al.* (ATLAS Collaboration), Phys. Rev. D **101**, 012002 (2020).
[55] N. M. Coyle, B. Li, and C. E. M. Wagner, Phys. Rev. D **97**, 115028 (2018).
[56] H. E. Haber and R. Hempfling, Phys. Rev. D **48**, 4280 (1993).
[57] M. Carena, J. R. Espinosa, M. Quiros, and C. E. M. Wagner, Phys. Lett. B **355**, 209 (1995).
[58] R. Harnik, G. D. Kribs, D. T. Larson, and H. Murayama, Phys. Rev. D **70**, 015002 (2004).
[59] S. Chang, C. Kilic, and R. Mahbubani, Phys. Rev. D **71**, 015003 (2005).
[60] A. Delgado and T. M. P. Tait, J. High Energy Phys. 07 (2005) 023.
[61] H. Georgi, A. Manohar, and G. W. Moore, Phys. Lett. **149B**, 234 (1984).
[62] H. Georgi and L. Randall, Nucl. Phys. **B276**, 241 (1986).
[63] M. A. Luty, Phys. Rev. D **57**, 1531 (1998).
[64] A. G. Cohen, D. B. Kaplan, and A. E. Nelson, Phys. Lett. B **412**, 301 (1997).
[65] G. F. Giudice and A. Masiero, Phys. Lett. B **206**, 480 (1988).
[66] G. F. Giudice and R. Rattazzi, Nucl. Phys. **B511**, 25 (1998).
[67] D. Dicus, A. Stange, and S. Willenbrock, Phys. Lett. B **333**, 126 (1994).
[68] N. Craig, F. D'Eramo, P. Draper, S. Thomas, and H. Zhang, J. High Energy Phys. 06 (2015) 137.
[69] S. Jung, J. Song, and Y. W. Yoon, Phys. Rev. D **92**, 055009 (2015).
[70] S. Gori, I. W. Kim, N. R. Shah, and K. M. Zurek, Phys. Rev. D **93**, 075038 (2016).
[71] M. Carena and Z. Liu, J. High Energy Phys. 11 (2016) 159.
[72] M. Aaboud *et al.* (ATLAS Collaboration), J. High Energy Phys. 01 (2018) 055.
[73] A. M. Sirunyan *et al.* (CMS Collaboration), J. High Energy Phys. 09 (2018) 007.
[74] E. Bagnaschi *et al.*, Eur. Phys. J. C **79**, 617 (2019).
[75] U. Ellwanger, J. F. Gunion, and C. Hugonie, J. High Energy Phys. 02 (2005) 066.
[76] J. L. Hewett, Phys. Rev. Lett. **70**, 1045 (1993).
[77] M. Misiak *et al.*, Phys. Rev. Lett. **114**, 221801 (2015).
[78] M. Misiak, Acta Phys. Pol. B **48**, 2173 (2017).
[79] M. Misiak and M. Steinhauser, Eur. Phys. J. C **77**, 201 (2017).
[80] R. Barbieri and G. F. Giudice, Phys. Lett. B **309**, 86 (1993).
[81] G. Degrassi, P. Gambino, and G. F. Giudice, J. High Energy Phys. 12 (2000) 009.
[82] M. Carena, D. Garcia, U. Nierste, and C. E. M. Wagner, Phys. Lett. B **499**, 141 (2001).
[83] A. J. Buras, P. H. Chankowski, J. Rosiek, and L. Slawianowska, Nucl. Phys. **B659**, 3 (2003).
[84] F. Gabbiani, E. Gabrielli, A. Masiero, and L. Silvestrini, Nucl. Phys. **B477**, 321 (1996).
[85] H. Arason, D. Castano, B. Keszthelyi, S. Mikaelian, E. Piard, P. Ramond, and B. Wright, Phys. Rev. Lett. **67**, 2933 (1991).
[86] M. Carena, S. Pokorski, and C. E. M. Wagner, Nucl. Phys. **B406**, 59 (1993).
[87] W. A. Bardeen, M. Carena, S. Pokorski, and C. E. M. Wagner, Phys. Lett. B **320**, 110 (1994).
[88] B. C. Allanach and S. F. King, Phys. Lett. B **328**, 360 (1994).
[89] M. Carena, S. Pokorski, and C. E. M. Wagner, Nucl. Phys. **B406**, 59 (1993).
[90] R. Hempfling, Phys. Rev. D **49**, 6168 (1994).
[91] L. J. Hall, R. Rattazzi, and U. Sarid, Phys. Rev. D **50**, 7048 (1994).
[92] M. Carena, M. Olechowski, S. Pokorski, and C. E. M. Wagner, Nucl. Phys. **B426**, 269 (1994).
[93] P. Langacker and N. Polonsky, Phys. Rev. D **49**, 1454 (1994).
[94] P. Langacker and N. Polonsky, Phys. Rev. D **50**, 2199 (1994).
[95] B. Schrempp, Phys. Lett. B **344**, 193 (1995).
[96] C. F. Kolda, L. Roszkowski, J. D. Wells, and G. L. Kane, Phys. Rev. D **50**, 3498 (1994).
[97] W. A. Bardeen, C. T. Hill, and M. Lindner, Phys. Rev. D **41**, 1647 (1990).
[98] T. E. Clark, S. T. Love, and W. A. Bardeen, Phys. Lett. B **237**, 235 (1990).
[99] M. Carena, T. E. Clark, C. E. M. Wagner, W. A. Bardeen, and K. Sasaki, Nucl. Phys. **B369**, 33 (1992).
[100] S. Komine and M. Yamaguchi, Phys. Rev. D **65**, 075013 (2002).
[101] J. Sato, K. Tobe, and T. Yanagida, Phys. Lett. B **498**, 189 (2001).
[102] C. Balazs and R. Dermisek, J. High Energy Phys. 06 (2003) 024.
[103] D. Auto, H. Baer, C. Balazs, A. Belyaev, J. Ferrandis, and X. Tata, J. High Energy Phys. 06 (2003) 023.
[104] H. Baer, I. Gogoladze, A. Mustafayev, S. Raza, and Q. Shafi, J. High Energy Phys. 03 (2012) 047.
[105] G. C. Branco, P. M. Ferreira, L. Lavoura, M. N. Rebelo, M. Sher, and J. P. Silva, Phys. Rep. **516**, 1 (2012).